Journal of Electronic Materials (2022) 51:1639–1652
https://doi.org/10.1007/s11664-022-09428-7

ORIGINAL RESEARCH ARTICLE

Growth and Characterization of Organic 2,4-Dinitroaniline Single Crystals for Optical Applications

S. Prince[1,2] · T. Suthan[2,3] · C. Gnanasambandam[2,4]

Received: 22 August 2021 / Accepted: 3 January 2022 / Published online: 24 January 2022

Abstract

Organic 2,4-dinitroaniline single crystals were successfully grown by slow evaporation solution growth technique. Single-crystal and powder X-ray diffraction studies were used to confirm the crystal structure. Fourier transform infrared (FTIR) and FT-Raman spectral analyses confirmed the presence of various functional groups in the grown crystal. The UV-Vis-NIR studies show that the cut-off wavelength is around 447 nm. The optical parameters such as optical band gap, Urbach energy, steepness parameter and electron-phonon interaction were calculated. The photoluminescence studies show green light emission. The thermogravimetric and differential thermal analyses expose the melting and decomposition points of the grown 2,4-dinitroaniline single crystal. The kinetic parameters such as the activation energy, frequency factor, entropy, enthalpy and Gibbs free energy were calculated by Coats Redfern and Horowitz-Mertzger methods. The dielectric studies were analyzed by the parallel plate capacitor method using the Agilent LCR meter. The electrical parameters such as plasma energy, Penn gap and Fermi energy of the grown single crystal were calculated. The third-order nonlinear optical properties of 2,4-dinitroaniline were measured using the Z-scan technique, with a 532-nm diode-pumped continuous wave (CW) Nd:YAG laser.

Graphical Abstract

2,4-dinitroaniline single crystal

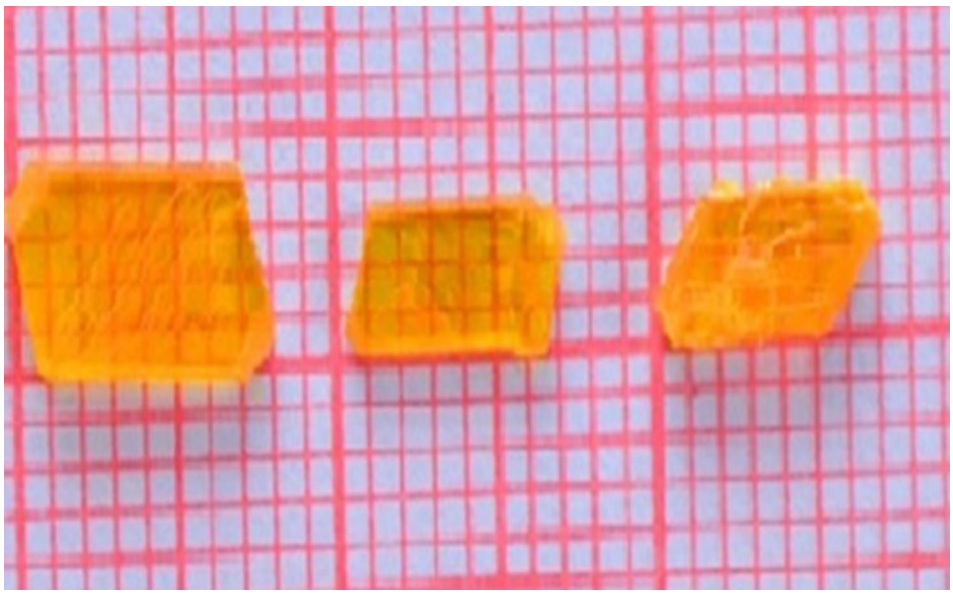

Keywords Organic compounds · crystal growth · optical properties · thermal properties · dielectric studies · nonlinear optical studies

Extended author information available on the last page of the article

Introduction

Organic molecular materials have attracted increased interest because of the unique prospects for fundamental research and practical applications. In recent years, the material industries have been searching for novel nonlinear optical materials. Organic nonlinear optical (NLO) materials are used in laser technologies, light-emitting diodes, transistors, conductors, electronic materials, optical circuits, optical communication, optical data storage technologies, optical signal processing, color displays, frequency doubling, integrated optics, photonic applications, electro-optic modulators and electro-optic switches.[1–4] Organic materials have good optical nonlinearity, chemical flexibility, thermal stability and excellent transmittance in the UV–visible regions. The optical properties of materials must be studied to determine their suitability for optoelectronic, photovoltaic applications and devices.[5] Mainly, the organic materials are soft, susceptible to breakage and budget-friendly. Organic aniline and its structures are highly studied because of their worth in many pharmaceuticals, electro-optical and other social applications. Aniline is an important raw material for producing dyes, oil paints, rubber and plastics. It is also widely used in electrical conduction, electroluminescence, rechargeable batteries and anticorrosion applications.[6–8] The nitro-substituted anilines have both donor (NH_2) and acceptor group (NO_2) hydrogen-bonding interactions. They are used in the design of supramolecular structures. The origin of their NLO responses was established to connect a large hyperpolarizability of the molecular π electron clouds.[9] Electronic absorption and emission spectra of nitroanilines depend on the closeness of the lowest-energy excited state and triplet states of character n–π^* and π–π^*.[10] The 2,4-dinitroaniline is a non-hygroscopic organic compound, and its molecular formula is $C_6H_5N_3O_4$. In the present work, organic 2,4-dinitroaniline single crystals were successfully grown by slow evaporation solution growth technique. The grown 2,4-dinitroaniline crystals were characterized by single-crystal XRD, powder XRD, FTIR and FT-Raman spectroscopy, optical, thermal, dielectric and third-order nonlinear optical analyses.

Experimental

The organic material 2,4-dinitroaniline was commercially purchased from Sigma Aldrich with 99% purity. The 2,4-dinitroaniline single crystal was grown by slow evaporation solution growth technique. The solubility was analyzed by the gravimetric method. Organic solvents, methanol, ethanol and acetone, were used to analyze the solubility. Finally, acetone was chosen as the best solvent to grow the 2,4-dinitroaniline single crystal. The solubility was analyzed in the temperature range from 30°C to 45°C as shown in Fig. 1. The figure reveals that as the temperature increases, solubility also increases. To obtain a homogeneous position, the solution was continuously stirred for 6 h. The solution was filtered and covered tightly with a perforated polyethylene cover to avoid dust particles in the environment and monitored constantly for nucleation events. Fine good-quality 2,4-dinitroaniline single crystals were harvested. The quality of the crystals was improved by successive recrystallization processes. The photograph of the grown 2,4-dinitroaniline single crystal is shown in Fig. 2.

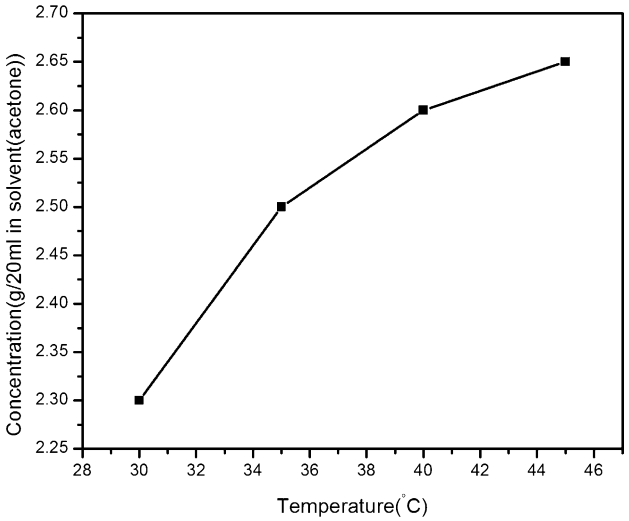

Fig. 1 Solubility curve of the 2,4-dinitroaniline single crystal.

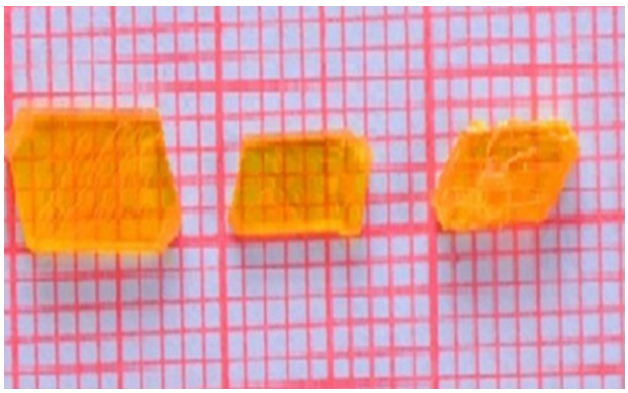

Fig. 2 Photograph of the 2,4-dinitroaniline single crystal.

Results and Discussion

X-ray Diffraction Studies

The crystallographic parameters of the grown 2,4-dinitroaniline were analyzed using a Bruker APEX II single-crystal X-ray diffractometer with MoK_{α} ($\lambda = 0.717073$ Å) radiation. The result shows that the grown 2,4-dinitroaniline single crystal belongs to the monoclinic crystal system with the centrosymmetric space group $P2_1/m$. The observed values are shown in Table I. The obtained values are well in agreement with the literature values.[11]

The powder X-ray diffraction studies of the grown 2,4-dinitroaniline crystal are analyzed by using an XPERT PRO diffractometer with Cuk_{α} (1.54060 Å) radiation with sample scanning speed of 1° min^{-1} and scanning angle ranging from 10° to 80°. The recorded powder XRD pattern of the 2,4-dinitroaniline single crystal is shown in Fig. 3. High-intensity sharp peaks are obtained and indicate the good crystalline nature of the grown crystal. The corresponding hkl values are indexed. The observed (*h k l*) values were in good agreement with the JCPDS file.[12]

FTIR and FT-Raman Spectral Studies

FTIR and FT-Raman spectral studies are used to identify the functional groups of the grown crystal. The FTIR spectrum was analyzed by using a PEIR SUBTECH SPECTRUM ASCII PEDS 4.00 spectrophotometer. The FTIR spectrum was recorded in the range of 4000-400 cm^{-1}. The obtained FTIR spectrum of the 2,4-dinitroaniline single crystal is shown in Fig. 4. The FT-Raman spectrum was analyzed using a BRUKER-RFS 27 FT-Raman spectrometer. The FT-Raman spectrum was recorded within the range of 3500-50 cm^{-1}. The obtained FT-Raman spectrum of the 2,4-dinitroaniline single crystal is shown in Fig. 5. The peaks observed at 3335 cm^{-1} and 3449 cm^{-1} are associated with symmetric and asymmetric stretching modes of the free NH_2 group in the FTIR spectrum. The absorption peak at 3330 cm^{-1} in the FT-Raman spectrum is attributed to symmetric stretching modes of the free NH_2 group. The peaks observed at 1425 cm^{-1} in FTIR and 1431 cm^{-1} in FT-Raman spectra are assigned to N-O asymmetric stretching. The peaks observed at 3063 cm^{-1} in FTIR and 3085 cm^{-1} in FT-Raman spectra are assigned as C-H stretching. The peaks observed at 1540 cm^{-1} in FTIR and 1520 cm^{-1} in FT-Raman spectra are assigned as C-C stretching. The peaks observed at 1629 cm^{-1} in the FTIR spectrum and the peak observed at 1619 cm^{-1} in the FT-Raman spectrum are attributed to NH_2 scissoring. The peak observed at 1259 cm^{-1} in the FTIR spectrum and 1249 cm^{-1} in the FT-Raman spectrum are attributed to the C-N stretching. The peak observed at 1374 cm^{-1} in the FTIR spectrum, and the peak observed at

Table I Single crystal XRD data for grown 2,4-dinitroaniline single crystal

Parameters	Literature	Present study
a (Å)	8.46	8.07
b (Å)	12.50	12.79
c (Å)	7.4	7.52
α (°)	90	90
β (°)	101.54	108.30
γ (°)	90	90
System	Monoclinic	Monoclinic
Space group	$P2_1/m$	$P2_1/m$

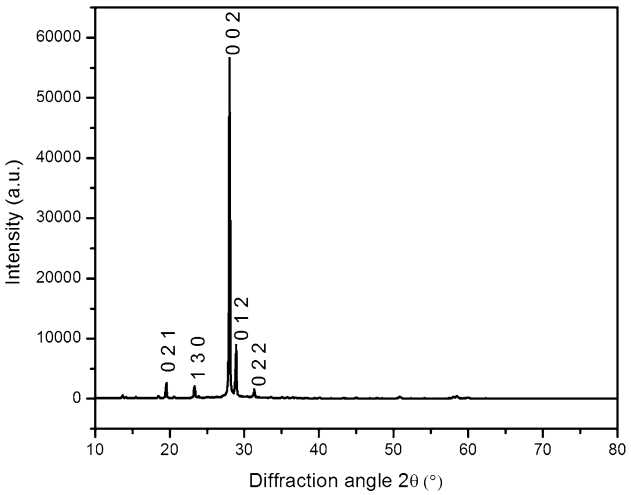

Fig. 3 Powder x-ray diffraction pattern of the 2,4-dinitroaniline single crystal.

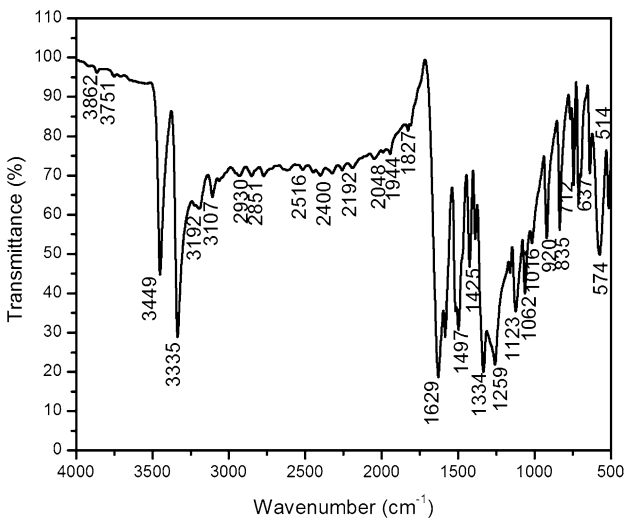

Fig. 4 FTIR spectrum of the 2,4-dinitroaniline single crystal.

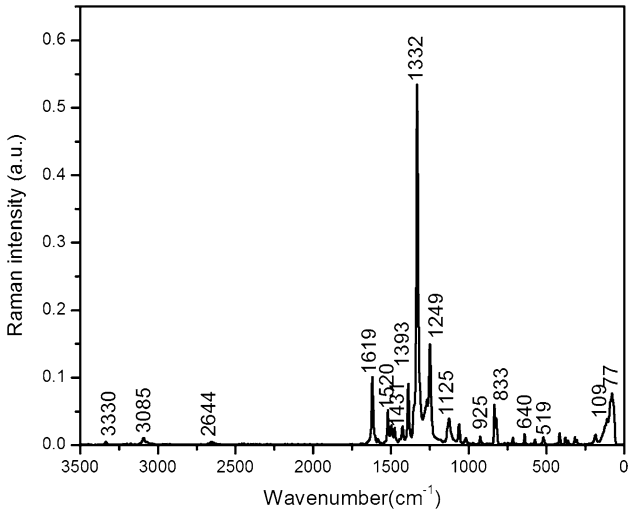

Fig. 5 FT-Raman spectrum of the 2,4-dinitroaniline single crystal.

1393 cm^{-1} in the FT-Raman spectrum are assigned as NO_2 symmetric stretching.

UV-Vis-NIR Studies

Studying the optical properties of materials is essential to evaluate the application of this material in optical data storage, optical devices, optoelectronics and photovoltaics.[13] Organic nonlinear optical single crystals are primarily used in optical applications where optical transmission range, transparency and cut-off wavelength are essential considerations.[14,15] The linear optical studies of the grown 2,4-dinitroaniline single crystal have been carried out by UV–Vis-NIR measurements in the range of 200-1100 nm using a Perkin–Elmer Lamda 35 spectrometer. The recorded transmittance spectrum of the 2,4-dinitroaniline single crystal is shown in Fig. 6a. The result reveals that the cut-off wavelength is around 447 nm and the grown 2,4-dinitroaniline single crystal has good transmittance in the visible and near-IR regions.

The absorption coefficient (α) has been calculated from the measured transmittance (T) using the formula

$$\alpha = \left(\frac{2.3026 \log\left(\frac{1}{T}\right)}{t} \right)$$

where t is the thickness of the sample.

Tauc's plot is used to measure the optical band gap (E_g) by the formula

$$(\alpha h\upsilon) = A(h\nu - E_g)^m$$

where h is Planck's constant, ν is the frequency of incident photons, A is a constant, E_g is the energy band gap and m is the index, which can have different values (2, 3, 1/2 and 3/2) corresponding to indirect allowed, indirect forbidden, direct allowed and direct forbidden transitions, respectively[16,17]

Taking the logarithm on both sides and differentiating the above band gap equation can also be written as[18]

$$\ln(\alpha h\nu) = \ln(A) + m\ln\left(h\nu - E_g\right)$$

$$\frac{d[\ln(\alpha h\nu)]}{d[h\nu]} = \frac{m}{h\nu - E_g}$$

The type of optical transition curve was formulated between $\frac{d[\ln(\alpha h\nu)]}{d[h\nu]}$ and $h\upsilon$ demonstrated a discontinuity at a particular value of $h\upsilon = E_g$. This discontinuity in a specific energy value gives a single transition and indicates the E_g value.[19,20] A graph was plotted for $\ln(\alpha h\upsilon)$ versus $\ln(h\upsilon - E_g)$, which is shown in Fig. 6b. The value of $m = ½$ was obtained from the slope of the curve. The optical transition of the 2,4-dinitroaniline single crystal has a direct allowed band gap nature. In a direct allowed transition, without a change in momentum (wave vector), the electron is simply relocated vertically from the top of the valence band to the bottom of the conduction band. Thus, to calculate the optical band gap, we can plot $(\alpha h\nu)^2$ versus $h\nu$ and extrapolate the linear portion of the curves until they intercept the photon energy axis. The optical band gap value of the grown 2,4-dinitroaniline single crystal is 2.59 eV obtained from Fig. 6c.

The extinction coefficient (K) is calculated as[21]

$$K = \frac{\lambda\alpha}{4\pi}$$

The extinction coefficient versus wavelength of the 2,4-dinitroaniline single crystal is shown in Fig. 6d. The transmittance (T) is calculated by[22]

$$T = \frac{(1-R)^2 \exp(-\alpha t)}{1 - R^2 \exp(-2\alpha t)}$$

The reflectance (R) in terms of the absorption coefficient is calculated by

$$R = \frac{\exp(-\alpha t) \pm \sqrt{\exp(-\alpha t)T - \exp(-3\alpha t)T + \exp(-2\alpha t)T^2}}{\exp(-\alpha t) + \exp(-2\alpha t)T}$$

The refractive index (n) is calculated by using the equation

$$n = \frac{-(R+1) \pm 2\sqrt{R}}{(R-1)}$$

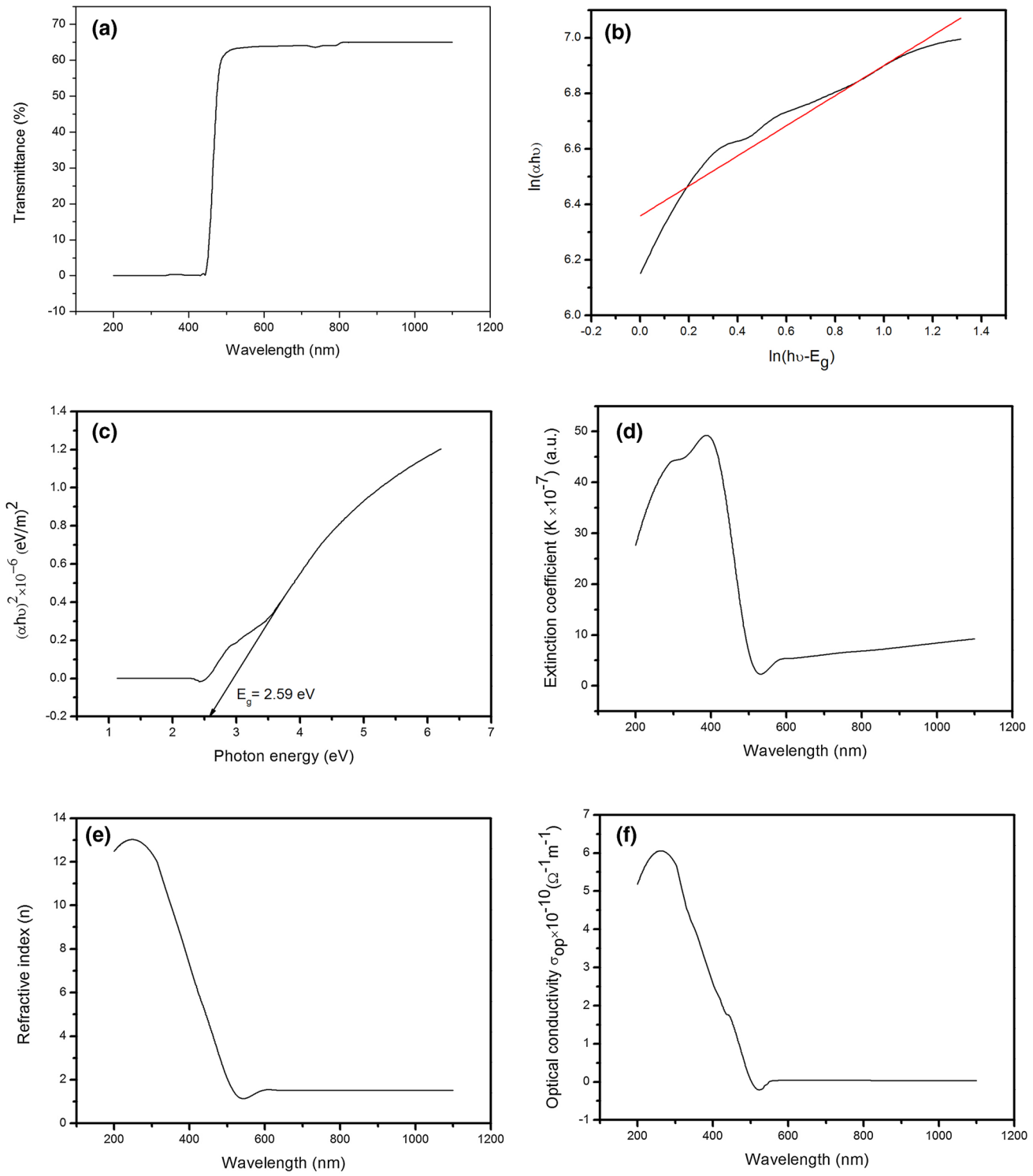

Fig. 6 (a) UV-Vis-NIR spectrum of the 2,4-dinitroaniline single crystal. (b) Plot of ln(αhν) versus ln(hν-E_g) for the 2,4-dinitroaniline single crystal. (c) Tauc's plot of $(\alpha h\nu)^2$ versus photon energy for the 2,4-dinitroaniline single crystal. (d) Extinction coefficient versus wavelength of the 2,4-dinitroaniline single crystal. (e) Plot of refractive index versus wavelength for the 2,4-dinitroaniline single crystal. (f) Optical conductivity versus wavelength of the 2,4-dinitroaniline single crystal. (g) Skin depth versus wavelength of the 2,4-dinitroaniline single crystal. (h) Plot of ln (α) versus photon energy of the 2,4-dinitroaniline single crystal.

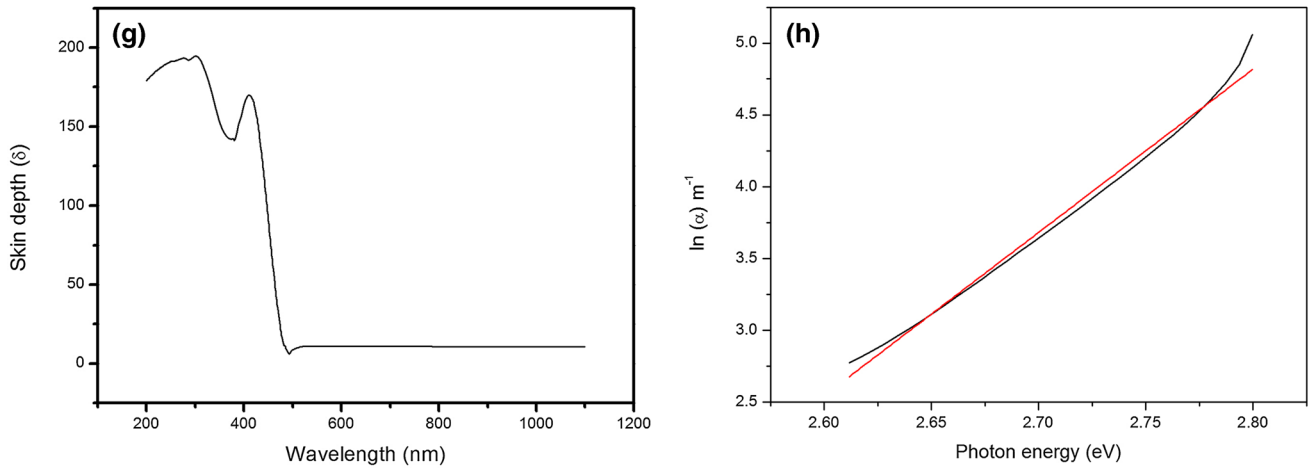

Fig. 6 (continued)

The refractive index versus wavelength of the 2,4-dinitroaniline crystal is shown in Fig. 6e. The optical conductivity is calculated by using the formula

$$\sigma_{op} = \frac{\alpha nc}{4\pi}$$

where c is the velocity of light. The graph plotted for the optical conductivity versus wavelength is shown in Fig. 6f.

The skin depth (δ) is numerically defined as

$$\delta = \frac{1}{\alpha}$$

The graph drawn for the skin depth versus wavelength for the 2,4-dinitroaniline single crystal is shown in Fig. 6g. The figure reveals that the skin depth is decreasing while moving towards high wavelength regions.

The Urbach energy (E_U) associated with the width of the Urbach tail obeys the exponential equation[23]

$$\alpha = \alpha_0 \exp\left(\frac{h\nu}{E_U}\right)$$

where α is the optical absorption coefficient and α_0 is a constant, hυ denotes the photon energy and E_U is the Urbach energy. The graph drawn for ln(α) versus hυ is shown in Fig. 6h. From the figure, the Urbach energy is calculated from the inverse slope. The calculated Urbach energy (E_U) of the 2,4-dinitroaniline single crystal is 0.0879 eV, which indicates less disorder and high crystallinity of the grown crystal.

The steepness parameter (σ) can be evaluated using the formula

$$\sigma = \left(\frac{k_B T}{E_U}\right)$$

Table II Linear optical parameters of the 2,4-dinitroaniline single crystal

Parameters	Calculated values
Optical band gap (E_g)	2.77 eV
Constant (α_o)	−27.0115 m^{-1}
Urbach energy (E_U)	0.0879 eV
Steepness parameter (σ)	0.2675
Electron-Phonon interaction ($E_{e\text{-}p}$)	2.491

where k_B is the Boltzmann constant in eV/K and T is the absolute temperature. The value of σ was found to be 0.2675. Electron-phonon interaction ($E_{e\text{-}p}$) is calculated by using the relation[24,25]

$$E_{e-p} = \frac{2}{3\sigma}$$

The strength of the electron-phonon interaction ($E_{e\text{-}p}$) is calculated as 2.491. The optical band gap energy (E_g), Urbach energy (E_U), steepness parameter (σ) and the electron-phonon interaction energy ($E_{e\text{-}p}$) are shown in Table II.

Photoluminescence Studies

The photoluminescence studies of the grown 2,4-dinitroaniline single crystal were recorded by using a spectrofluorometer with a 450 W high-pressure Xenon lamp as an excitation source. The grown 2,4-dinitroaniline single crystal is excited at 466 nm. The obtained emission spectrum is shown in Fig. 7. The high-intensity peak observed at 532 nm is attributed to the n–π^* transition. The result indicates that the grown 2,4-dinitroaniline single crystal exhibits green-light emission, which may be useful for new green colour emitting material.

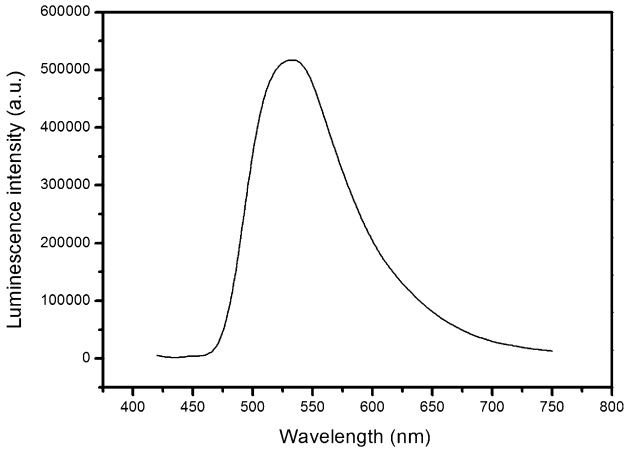

Fig. 7 Photoluminescence spectrum of the 2,4-dinitroaniline single crystal.

Thermal Analysis

The thermal properties of the grown 2,4-dinitroaniline single crystal were determined by thermogravimetric (TG) and the differential thermal analyses (DTA) using a Perkin Elmer Diamond TG/DTA analyzer with a heating rate of 10°C/min in a nitrogen atmosphere. The TG/DTA curve of the 2,4-dinitroaniline single crystal is shown in Fig. 8a. In the DTA analysis, the peak observed around 180°C is assigned as the melting point of the grown 2,4-dinitroaniline single crystal. In DTA analysis, the peak observed around 345°C may be assigned as the decomposition point of the 2,4-dinitroaniline single crystal. In this stage, heavy weight loss in TGA has been noted. In TGA analysis, the single-stage weight loss curve occurs and it was stable up to 200°C. The kinetic parameters were calculated using Coats–Redfern and Horowitz-Metzger methods.[26,27] The order of reaction ($n = 1$) is used in the present investigation. For the determination of activation energy, Coats–Redfern derived the equation

$$\ln\left[\frac{-ln(1-\alpha)}{T^2}\right] = ln\left[\left(\frac{ZR}{\beta E}\right)\left(1-\frac{2RT}{E}\right)\right] - \frac{E}{RT}$$

where α is the fractional mass loss, T is the absolute temperature, Z is the pre-exponential factor, R is the gas constant ($R = 8.317$ Jmol^{-1} K^{-1}), β is the heating rate and E is the activation energy. The value of α is equal to the total mass loss up to a particular temperature divided by total mass loss in the step involved.

$$\alpha = \frac{Wo - W}{W_o - W_f}$$

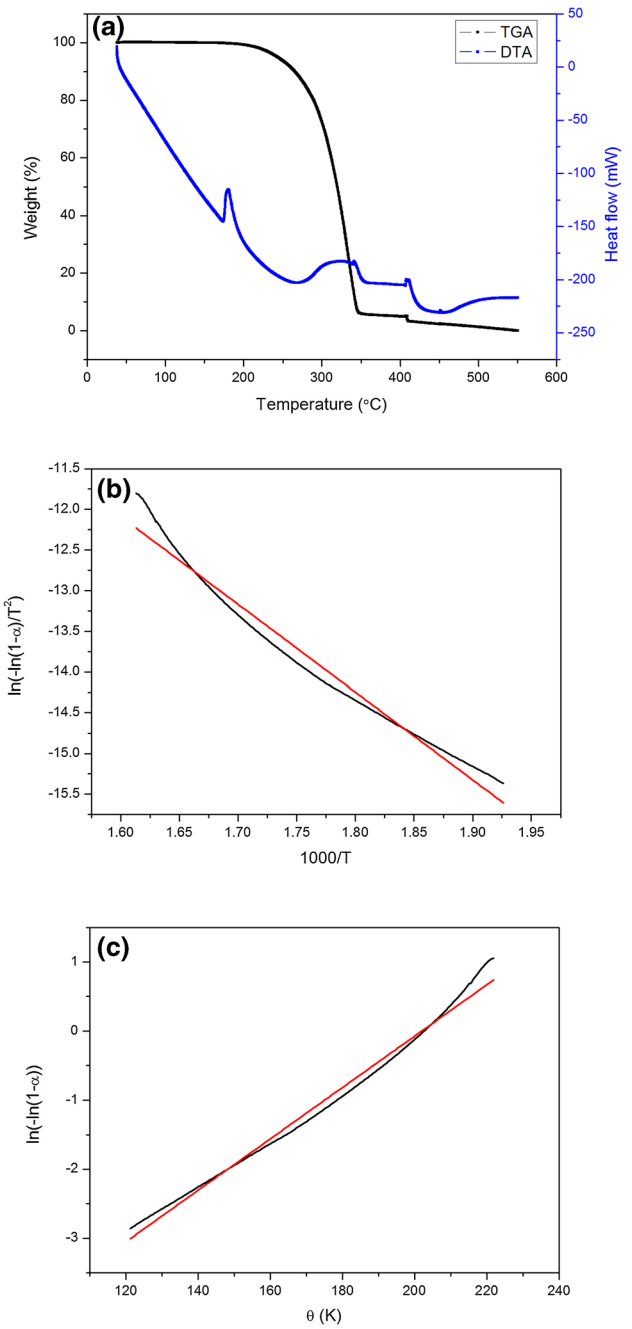

Fig. 8 (a) TG/DTA curves of the 2,4-dinitroaniline single crystal. (b) Coats-Redfern plot for the 2,4-dinitroaniline single crystal. (c) Horowitz-Metzger plot for the 2,4-dinitroaniline single crystal.

where W_0 is the initial weight, W is the actual weight at any degradation time, W_f is the final weight at the end of the thermal degradation process. In the Coats-Redfern equation, the activation energy is calculated from plot of $ln\left[\frac{-ln(1-\alpha)}{T^2}\right]$ versus 1000/T, and it is shown in Fig. 8b. From the slope,

the value of activation energy is calculated. Horowitz and Metzger derived an equation for extracting pyrolysis parameters by using TGA. The first-order reaction developed the following equation.[27–30]

$$\ln\left[-\ln\left(1-\alpha\right)\right]=\frac{E\theta}{RT_m^2}$$

$$\theta = T - T_m$$

where T_m is the temperature of maximum reaction rate and T is the temperature in Kelvin at any instant. According to this method, a plot of ln[−ln(1−α)] versus temperature gives the activation energy of degradation. The plot of ln[−ln(1−α)] versus θ give the best linear fit and is shown in Fig. 8c. The slope, intercept, E and Z values are calculated from Fig. 8b and c and the mechanisms are evaluated. The enthalpy of activation, ΔH^*, is evaluated from the equation

$$\Delta H^* = E - RT$$

Gibbs free energy ΔG^* is calculated from the equation

$$\Delta G^* = \Delta H^* - T\Delta S$$

The entropy of activation ΔS^* in ($JK^{-1}mol^{-1}$) is evaluated from the equation

$$Z=\left(\frac{kT_m}{h}\right)\exp\left(\frac{\Delta S^*}{R}\right)$$

where h is Planck's constant, k is the Boltzmann constant. The calculated enthalpy value is positive. The positive value of enthalpy indicates that the process was endothermic.[31–39] The activation entropy has negative values, which shows that the decomposition reactions proceed with a lower rate than normal ones. The negative value of entropy also shows the more ordered structure of the 2,4-dinitroaniline single crystal than the reactants. The entropy of activation increases with the increase of activation energy. The positive value of ΔG^* shows that the reaction involved in the decomposition of the 2,4-dinitroaniline single crystal is not spontaneous. The calculated kinetic parameter values are shown in Table III.

Table III Kinetic parameters for the 2,4-dinitroaniline single crystal

Kinetic parameters	Coats–Redfern	Horowitz-Metzger
Activation energy, E (kJ mol^{-1})	89.67672	78.25073
Frequency factor, Z (s^{-1})	8.94E+06	2.35E+07
Entropy, ΔS^* (J K^{-1} mol^{-1})	−12.70	−108.16
Enthalpy, ΔH^* (kJ mol^{-1})	85.49	74.07
Gibbs free energy, ΔG^* (kJ mol^{-1})	91.90	128.47

Dielectric Studies

The dielectric properties of the grown 2,4-dinitroaniline single crystal was analyzed by an Agilent 4284A LCR Meter using the conventional parallel plate capacitor method.[40–42] The capacitance (C_{crys}) and dielectric loss (tan δ) were measured at several temperatures ranging from 313 K to 383 K with a frequency range of 1 kHz to 1 MHz. The cut and polished transparent single crystals are used inside the parallel plates of the condenser for dielectric measurements. The dielectric constant of the grown crystal was calculated using the following relation

$$\varepsilon_r=\left(\frac{A_{air}}{A_{crys}}\right)\left(\frac{C_{crys}-C_{air}\left(1-\frac{A_{crys}}{A_{air}}\right)}{C_{air}}\right)$$

where A_{air} is the area of electrode, A_{crys} is the area of crystal, C_{crys} is the capacitance of the crystal and C_{air} is the air capacitance. The AC conductivity (σ_{ac}) was found using the relation

$$\sigma_{ac} = \varepsilon_0\varepsilon_r\omega\tan\delta$$

The temperature dependence of the dielectric constant (ε_r), dielectric loss (tan δ) and AC conductivity (σ_{ac}) at different frequencies are shown in Fig. 9a, b and c. From the figure, the dielectric constant, the dielectric loss and the AC conductivity increase with the increase in temperature. The dielectric constant and dielectric loss values decrease with increased frequency, but the AC conductivity value increases with increased frequency. The results show that the grown 2,4-dinitroaniline single crystal has normal dielectric behaviour. The low dielectric loss with high frequency shows that the grown 2,4-dinitroaniline crystal maintains good optical quality with fewer defects. In dielectric material, the activation energy (E_a) is also measured at room temperature and it obeys the Arrhenius law[43]

$$\sigma_{ac} = \sigma_0\exp\left(-E_a/kT\right)$$

where σ_0 is the pre-exponent factor, E_a is the activation energy, k is the Boltzmann constant and T is the absolute temperature. The Arrhenius plot drawn as lnσ_{ac} versus 1000/T is shown in Fig. 9d. The activation energy of the 2,4-dinitroaniline single crystal is calculated at various frequencies (1 kHz, 10 kHz, 100 kHz and 1 MHz) and the obtained values are 0.3263 eV, 0.2932 eV, 0.1745 eV and 0.0819 eV. The above results show that when the frequency increases, the activation energy decreases, which may be attributed to an increase in field frequency, which

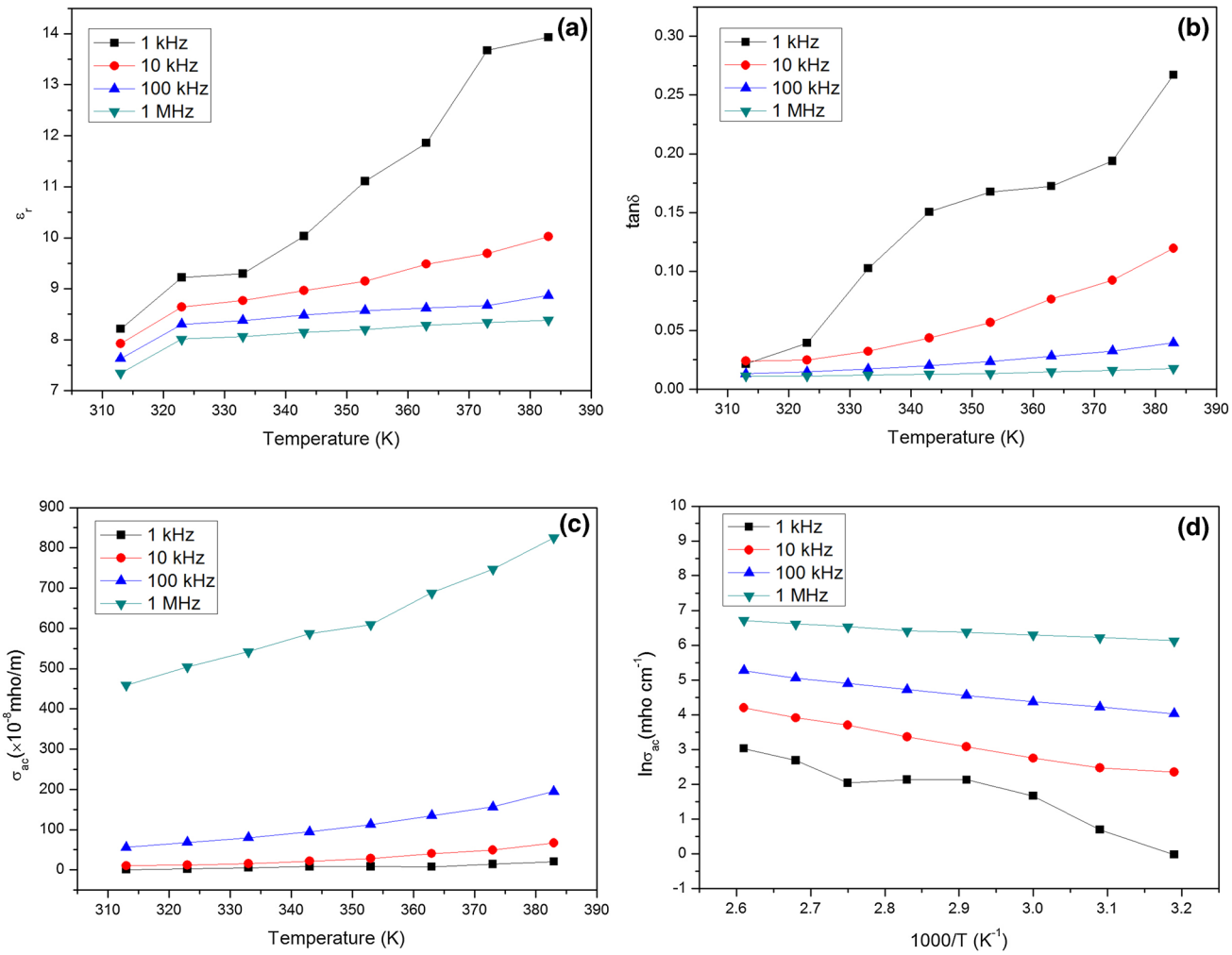

Fig. 9 (a) Dielectric constants observed for the 2,4-dinitroaniline single crystal. (b) Dielectric loss observed for the 2,4-dinitroaniline single crystal. (c) AC electrical conductivities observed for the 2,4-dinitroaniline single crystal. (d) Plot of lnσ_{ac} versus 1000/T for the 2,4-dinitroaniline single crystal.

is responsible for electronic jumps between the localized states. The dielectric measurement is a practical tool to evaluate the electronic polarizability of the grown 2,4-dinitroaniline single crystal. According to the Penn model, the average Penn gap (E_p) and Fermi energy (E_F) were evaluated by subsequent equations.[44] To calculate the valence electron plasma energy $\hbar\omega_p$, the following equation is used[45]

$$\hbar\omega_P = 28.8\left(\frac{Z\rho}{M}\right)^{1/2}$$

where $Z = (6\times Z_C) + (5\times Z_H) + (3\times Z_N) + (4\times Z_O)$ is the total number of valence electrons. The molecular weight (M) of the 2,4-dinitroaniline single crystal is 183.123 g/mol.

The density of the 2,4-dinitroaniline single crystal was evaluated by the formula

$$\rho = \frac{MZ}{N_a V}$$

where M is the molecular weight of the 2,4-dinitroaniline single crystal (M = 183.123 g/mol), Z is the molecular unit cell (Z = 4), N_a is Avogadro's number ($N_a = 6.023\times10^{23}$), V is the volume of the unit cell (V = 737 Å^3). The obtained density value of the 2,4-dinitroaniline single crystal is 1.65 gm^{-3}. The Penn gap is calculated by using the following relation

$$E_p = \frac{\hbar\omega_P}{\left(\varepsilon_r - 1\right)^{1/2}}$$

Fermi energy is calculated by the following formula

$$E_F = 0.2948\left(\hbar\omega_P\right)^{4/3}$$

where E_P is the Penn gap, E_F is the Fermi energy in eV, $\hbar\omega_p$ is the valence electron plasma energy and ε_r is the dielectric constant of the material at the frequency (1 kHz). The electronic polarizability (α) of the grown crystal is calculated by the formula[46]

$$\alpha = \left(\frac{\left(\hbar\omega_P\right)^2 S_0}{\left(\hbar\omega_P\right)^2 S_0 + 3E_P^2}\right) \times \frac{M}{\rho} \times 0.396 \times 10^{-24}\text{cm}^3$$

where S_0 is a constant for a particular material is given by

$$S_0 = 1 - \left(\frac{E_P}{4E_F}\right) + \frac{1}{3}\left(\frac{E_P}{4E_F}\right)^2$$

The Clausius-Mossotti relation is as follows

$$\alpha = \left(\frac{3M}{4\pi N_a \rho}\right)\left(\frac{\varepsilon_r - 1}{\varepsilon_r + 2}\right)$$

where N_a is the Avogadro number ($N_a = 6.023 \times 10^{23}$)

The following empirical relationship is used to calculate α

$\alpha = \left(1 - \frac{\sqrt{E_g}}{4.06}\right) \times \frac{M}{\rho} \times 0.396 \times 10^{-24}\ \text{cm}^3$ where E_g is the optical band gap (eV). The calculated electronic properties of plasma energy, Penn gap, Fermi energy and electronic polarizability for the 2,4-dinitroaniline single crystal values are shown in Table IV.

Nonlinear Studies

The third-order nonlinear optical properties of the grown 2,4-dinitroaniline were analyzed using Z-scan measurements. The grown sample is translated in the Z-direction in this method along the axis of the focused Gaussian beam from a continuous-wave 532-nm diode-pumped Nd:YAG laser beam spectrometer and the far-field intensity is

Table IV Electronic parameters for 2, 4-dinitroaniline single crystal

Parameter	Calculated values
Plasma energy ($\hbar\omega_p$)	22.2683 eV
Penn gap (E_P)	7.072 eV
Fermi energy (E_F)	16.654 eV
Electronic polarizability (α)	
From Penn analysis	3.368×10^{-23} cm^3
From Clausius Mossotti equation	3.462×10^{-23} cm^3
From optical band gap	2.681×10^{-23} cm^3

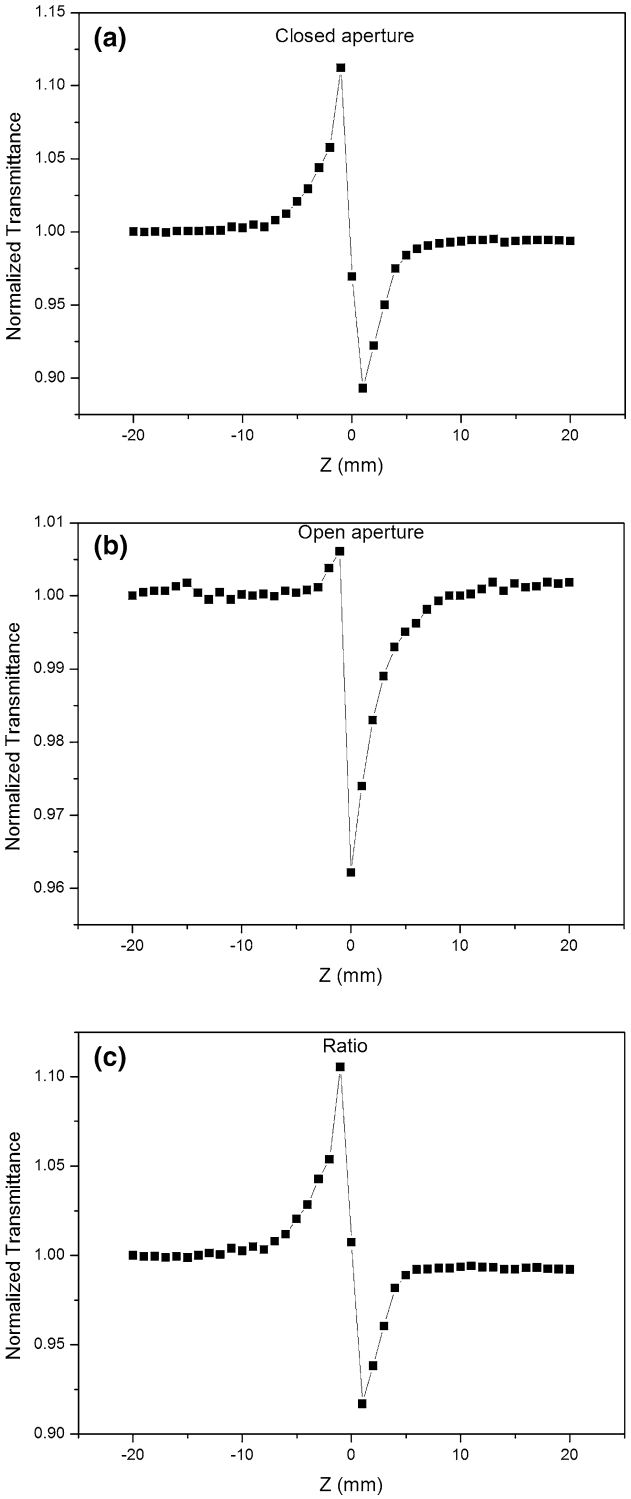

Fig. 10 (a) Closed-aperture Z-scan for the grown 2,4-dinitroaniline single crystal. (b) Open-aperture Z-scan for the grown 2,4-dinitroaniline single crystal. (c) Ratio of closed-to-open-aperture Z-scan for the grown 2,4-dinitroaniline single crystal.

measured as a function of the sample position. Two apertures (closed and open aperture) are used for the measurements of nonlinear refractive index (n_2) and nonlinear absorption coefficient (β).[47] The nonlinear optical coefficients n_2, β and $\chi^{(3)}$ were calculated using the standard equations.[48] Figure 10 (a–c) shows the closed and open scans, the ratio of the closed-to-open normalized Z-scan of the 2,4-dinitroaniline single crystal. The peak followed by a valley normalized transmittance acquired from the closed-aperture curve illustrates the self-defocusing effect.[49,50] In general, the nonlinear absorption was categorized into two properties. The sample transmittance increases with an increase in the optical intensity, which is termed saturation absorption (SA). The samples transmittance decreases while increasing the optical intensity is termed as reverse saturation absorption (RSA). The two-photon and multi-photon absorptions are arising due to the reverse saturation absorption.[50,51] The difference between the peak and valley transmission ($\Delta T_{p\text{-}v}$) is written in terms of the on-axis phase shift at the focus as

$$\Delta T_{p-v} = 0.406(1-S)^{0.25}\Delta\Phi o$$

where ΔΦo is the axis phase shift at the focus and it is given by

$$\Delta\Phi_0 = \frac{\Delta T_{p-v}}{0.406(1-S)^{0.25}}$$

S is the linear transmittance aperture. It can be calculated using the relation

$$S = 1 - exp\left(\frac{-2r_0^2}{\omega_0^2}\right)$$

where r_0 is the aperture radius and ω_0 is the beam radius at the aperture. The nonlinear absorption coefficient (β) is estimated from open-aperture Z-scan data[52–54]

$$\beta = \frac{2\sqrt{2}\Delta T}{I_0 L_{\text{eff}}}$$

$$L_{\text{eff}=[1-\exp(-\alpha L)]/\alpha}$$

where L_{eff} is the effective thickness of the sample, α is the linear absorption coefficient, L is the thickness of the sample, I_0 is the on-axis irradiance at the focus (3.47 KW/cm^2) and ΔT denotes the valley value from the Z-scan curve of open aperture (Fig. 10b).

The nonlinear refractive index (n_2) is calculated by using the relation

$$n_2 = \frac{\Delta\Phi_0}{kI_0L_{\text{eff}}}$$

where k is the wavenumber i.e. $k = 2\pi/\lambda$, $\Delta\Phi_0$ is the on-axis phase shift.

The real and imaginary parts of the third-order nonlinear optical susceptibility $\chi^{(3)}$ were determined using the following formula[48,55]

$$\text{Re}\chi^{(3)}(esu) = 10^{-4}\frac{\varepsilon_0 c^2 n_0^2}{\pi} n_2\left(\frac{cm^2}{W}\right)$$

$$I_m\chi^{(3)}(esu) = 10^{-2}\frac{\varepsilon_0 c^2 n_0^2 \lambda}{4\pi^2}\beta\left(\frac{cm}{W}\right)$$

where ε_o is the permittivity of free space, c is the velocity of light in free space, n_o is the linear refractive index of the sample. The third-order nonlinear optical susceptibility is calculated

$$\left|\chi^{(3)}\right| = \left[\left(R_e\left(\chi^{(3)}\right)\right)^2 + \left(I_m\left(\chi^{(3)}\right)\right)^2\right]^{1/2}$$

From the closed-aperture Z-scan curve, the prefocal transmittance peak is followed by the post-focal valley, which is the sign of negative nonlinearity.[56] As the material has a negative refractive index, it results in defocusing the nature of the material, which is an essential property for the application in the protection of optical sensors such as night vision devices.[57] A focal point, the beam waist diameter ($2\omega_o$) can be determined using the following equation[58]

$$\omega_0 = \frac{2\lambda}{\pi}\left(\frac{f}{d}\right)$$

where λ is the wavelength of the laser (532 nm), f is the focal length of the convex lens (103 mm) and d is the diameter of the laser beam (4 mm). The beam waist radius (ω_o) is found to be 8.73 µm. The thickness of the sample (L) was 1 mm (holder inner diameter). The factor of Rayleigh length was satisfied for this condition.

$$Z_R = \frac{\pi\omega_0^2}{\lambda}$$

Using the above formula, the Rayleigh length (Z_R) was calculated as 45 mm. The thickness of the sample must be less than the Rayleigh length, and it was satisfied ($L < Z_R$). Also, the second-order molecular hyperpolarizability (γ) of the grown 2,4-dinitroanline single crystal is related to the third-order bulk susceptibility as[59]

$$\gamma = \frac{\chi^3}{N^* f^4}$$

Table V Nonlinear parameters of the 2,4-dinitroaniline single crystal

Parameters	Measured values
Nonlinear refractive index (n_2)	1.34×10^{-15} cm^2/W
Nonlinear absorption coefficient (β)	3.61×10^{-9} cm/W
Real part of third-order susceptibility [R_e ($\chi^{(3)}$)]	7.97×10^{-14} esu
Imaginary part of third-order susceptibility [I_m ($\chi^{(3)}$)]	9.08×10^{-13} esu
Third order nonlinear susceptibility ($\chi^{(3)}$)	9.11×10^{-13} esu
Second order molecular hyperpolarizability (γ)	3.92×10^{-35} esu

The obtained γ was found to be 3.92×10^{-35} esu, where '*N**' is the number of molecules per cm^3 and '*f*' is the local-field correction factor. The value of *N** is obtained from the formula

$$N^* = \frac{\rho N_A}{M}$$

where ρ is the density of the sample, N_A is Avogadro number and M is the mass of the sample (183.123 g/mol) and it was found to be 5.30×10^{21} cm^{-3}.

According to the Lorentz equation,

$$f = \frac{\left(n_0^2 + 2\right)}{3},$$

The obtained f value is 1.44. The coupling factor (ρ*) is the ratio of the imaginary part [$I_m \chi^{(3)}$] to the real part [$R_e \chi^{(3)}$] of third-order nonlinear susceptibility

$$\rho^* = \frac{I_m \chi^{(3)}}{R_e \chi^{(3)}}$$

The value of ρ* was found to be 7.97×10^{-14}.

The crystal is suitable for optical switches if the conditions $W > 1$ and $T < 1$ are satisfied. W and T were evaluated by the formula[60,61]

$$W = \frac{n_2 I_0}{\alpha_0 \lambda}$$

$$T = \frac{\beta \lambda}{n_2}$$

where n_2 is the nonlinear refractive index, I_o is the irradiance of the laser beam, α_o is the linear absorption coefficient, β is the nonlinear absorption coefficient and λ *is* the wavelength of the laser source. The figures of merit were calculated to be $W= 9.4\times10^{-2}$ and T=1.43. Since the conditions for W and T were not satisfied, the grown 2,4-dinitroaniline single crystal is inappropriate for use in optical switching devices at a wavelength of 532 nm, but it may be used for applications of holographic recording and two-wave mixing.[61] Using the Z-scan technique, the calculated nonlinear parameter values of the 2,4-dinitroaniline single crystal with a 532-nm Nd:YAG laser are shown in Table V.

Conclusion

The organic 2,4-dinitroaniline single crystal was grown using acetone solvent by slow evaporation solution growth technique. The single-crystal and powder XRD studies show that the grown crystal belongs to a monoclinic crystal system with the centrosymmetric space group $P2_1/m$. FTIR and FT-Raman spectral studies confirmed functional groups of the grown 2,4-dinitroaniline single crystal. UV-Vis-NIR spectral analysis shows that the 2,4-dinitroaniline single crystal is transparent in the visible and near-IR regions and the cut-off wavelength is around 447 nm. Using Tauc's plot, the optical band gap was calculated as 2.59 eV. The photoluminescence analysis shows that the high-intensity peak observed around 532 nm exhibits green emission. The TG/DTA studies confirmed the melting and decomposition points of the grown 2,4-dinitroaniline single crystal as 180°C and 345°C, respectively. The values of kinetic parameters such as order of reaction (n), activation energy (E), frequency factor (Z), enthalpy (ΔH*), entropy (ΔS*) and Gibbs free energy (ΔG*) were calculated. The observed lower values of dielectric constant and dielectric loss of 2,4-dinitroaniline may be suitable for NLO applications. The electronic parameters such as plasma energy ($\hbar\omega_p$), Penn gap (E_P), Fermi energy (E_F) and polarizability (α) were calculated. The third-order nonlinear studies show that the grown 2,4-dinitroaniline single crystal exhibits negative optical nonlinearity.

Acknowledgments This work was supported by the University Grants Commission (UGC), South Eastern Regional Office (SERO), Government of India, under the grant of Minor Research Project UGC Reference No: F. MRP-7005/16 (SERO/UGC) Link No: 7005, is hereby gratefully acknowledged.

Conflict of interest The authors declare that they have no conflict of interest.

References

1. I. Sharma, and A.S. Hassanien, *J. Non Cryst. Solids.* 548, 120326 (2020).
2. P. Gunter, *Nonlinear Optical Effects and Materials* (Berlin: Springer-verlag, 2000).
3. S. Sun, and N.S. Sariciftci, *Organic Photovoltaics Mechanisms, Materials and Devices* (USA: CRC Press Taylor and Francis group, 2005).
4. I.M. El-Radaf, H.Y.S. Al-Zahrani, and A.S. Hassanien, *J. Mater. Sci. Mater. Electron.* 31, 8336 (2020).
5. A.S. Hassanien, I. Sharma, and K.A. Aly, *Physica B Condens. Matter.* 613, 412985 (2021).
6. C.T. Yan, T.S. Shih, and J.F. Jen, *J. Talanta.* 64, 650 (2004).

7. H.L. Wang, F. Huang, A.G.M. Diamid, Y.Z. Wang, and D.D. Gebler, *J. Epstein. Synth. Met.* 78, 33 (1996).
8. P. Novak, K. Muller, K.S.V. Santhanam, and O. Haas, *J. Chem. Rev.* 97, 207 (1997).
9. J. Zyss, *Molecular Nonlinear Optics: Materials Physics and Devices* (New York: Academic Press, 1994).
10. G.L. Findley, T.P. Carsey, and S.P. MeGlynn, *J. Am. Chem. Soc.* 101, 4511 (1979).
11. K.H.M. Mannan, M.B. Hossain, and M.D. Shamsuzzoha, *J. Acta Cryst. B.* 29, 2315 (1973).
12. JCPDS file card no: 97-02-9, 2θ 1792
13. A.S. Hassanien, I.M. El Radaf, and A.A. Akl, *J. Alloys Compd.* 849, 156718 (2020).
14. T. Suthan, P.V. Dhanaraj, N.P. Rajesh, C.K. Mahadevan, and G. Bhagavannarayana, *Cryst. Eng. Comm.* 13, 4018 (2011).
15. T. Suthan, N.P. Rajesh, C.K. Mahadevan, D. Sajan, and G. Bhagavannarayana, *Mater. Chem. Phys.* 130, 915 (2011).
16. A.S. Hassanien, R. Neffati, and K.A. Aly, *Optik* 212, 164681 (2020).
17. R.P. Jebin, T. Suthan, T.R. Anitha, N.P. Rajesh, and G. Vinitha, *J. Mater. Sci. Mater. Electron.* 32, 3232 (2021).
18. F. Yakuphanoglu, B.F. Senkal, and A. Sarac, *J. Electron. Mater.* 37, 930 (2008).
19. A. Dev, S. Chakrabarti, S. Kar, and S. Chaudhuri, *J. Nanopart. Res.* 7, 195 (2005).
20. S. Banerjee, A. Kumar, and J. NuclInstrum, *Methods Phys. Res. B.* 269, 2798 (2011).
21. B.K. Periyasamy, R.S. Jebas, N. Gopalakrishnan, and T. Balasubramanian, *Mater. Lett.* 61, 4246 (2007).
22. D.K. Schroder, *Semiconductor Material and Device Characterization* (New York: Wiley, 1990).
23. M. Zarrinkhameh, A. Zendehnam, S.M. Hosseini, N. Robatmili, and M. Arabzadegan, *J. Bull. Mater. Sci.* 37, 533 (2014).
24. A.S. Hassanien, and A.A. Akl, *J. Superlattices Microstruct.* 89, 153 (2016).
25. M. Karimi, M. Rabiee, F. Moztarzadeh, M. Tahriri, and M. Bodaghi, *J. Curr. Appl. Phys.* 9, 1263 (2009).
26. A.W. Coats, and J.P. Redfern, *J. Poly. Sci.* 3, 917 (1965).
27. H.H. Horowitz, and G. Metzger, *J. Anal. Chem.* 35, 1464 (1963).
28. A. Broido, *J. Polym. Sci.* 7, 1761 (1969).
29. K.K. Bamzai, and S. Kumar, *J. Mater. Chem. Phys.* 107, 200 (2008).
30. P.S. Abthagir, and R. Saraswathi, *J. Mater. Chem. Phys.* 92, 21 (2005).
31. S.H. Guzar, and Q.H. Jin, *J. Chem. Res. Chin. Univ.* 24, 143 (2008).
32. H.T.S. Britton, *Hydrogen Ions*, 3rd ed., (London: Chapman and Hall, 1942).
33. E. Karapmar, I.H. Gubbuk, B. Taner, P. Deveci, and E. Ozcan, *J. Chem.* 60, 997 (2013).
34. N. Mathur, S. Bargotya, and R. Mathur, *J. Appl. Chem.* 3, 712 (2014).
35. J.B. Devhade, *J. Appl. Chem.* 4, 1556 (2015).
36. M.R.R. Prasad, K.S. Babu, and B. Sreedhar, *J. Appl. Chem.* 4, 1757 (2015).
37. A. Chaudhary, and A. Singh, *J. Appl. Chem.* 5, 1038 (2016).
38. M. Sharma, S. Agarwal, and A. Mishra, *J. Appl. Chem.* 3, 1139 (2014).
39. P.P. Talware, and P.M. Yeole, *J. Appl. Chem.* 3, 902 (2014).
40. T. Suthan, N.P. Rajesh, P.V. Dhanaraj, and C.K. Mahadevan, *Spectrochim. Acta A Mol. Biomol. Spectrosc.* 75, 69 (2010).
41. T. Suthan, and N.P. Rajesh, *J. Cryst. Growth.* 312, 3156 (2010).
42. T. Suthan, N.P. Rajesh, C.K. Mahadevan, K.S. Kumar, and G. Bhagavannarayana, *Spectrochim. Acta A Mol. Biomol. Spectrosc.* 79, 1443 (2011).
43. L. Jentjens, N.L. Raeth, K. Peithmann, and K. Maier, *J. Appl. Phys.* 109, 121 (2011).
44. D.R. Penn, *J. Phys. Rev.* 128, 2093 (1962).
45. V. Kumar, and B.S.R. Sastry, *J. Phys. Chem. Solids.* 66, 99 (2005).
46. S.S.B. Solanki, N.P. Rajesh, and T. Suthan, *J. Mater. Sci. Mater. Electron.* 32, 1808 (2021).
47. R.K. Choubey, S. Medhekar, R. Kumar, S. Mukherjee, and S. Kumar, *J. Mat. Sci. Elect. Mat.* 25, 1410 (2014).
48. R.P. Jebin, T. Suthan, N.P. Rajesh, and G. Vinitha, *J. Opt. Laser Technol.* 115, 500 (2019).
49. M. Sheik-Bahae, A.A. Said, T. Wei, D.J. Hagan, and E.W. Van Stryland, *Sens. IEEE J. Quant. Elect.* 26, 760 (1990).
50. R.M. Jauhar, P. Vivek, K. Sudhakar, S. Kalainathan, M.N. Mohideen, and P. Murugakoothan, *J. Therm. Anal. Cal.* 124, 871 (2015).
51. P. Nagapandiselvi, C. Baby, and R. Gopalakrishnan, *J. RSC Adv.* 4, 22350 (2014).
52. M. Sheik-Bahae, A.A. Said, and E.W. Van Stryland, *J. Opt. Lett.* 14, 955 (1989).
53. E.W. Van Stryland, M. Sheik-Bahae, M.G. Kuzyk, C.W. Dirk (Eds.), Characterization Techniques and Tabulations for Organic Nonlinear Materials (Marcel DekkerInc, 1998)
54. T. Kanagasekaran, P. Mythili, P. Srinivasan, A.Y. Nooraldeen, P.K. Palanisamy, and R. Gopalakrishnan, *J. Cryst. Growth. Des.* 8, 2335 (2008).
55. V. Subashini, S. Ponnusamy, and C. Muthamizhchelvan, *J. Cryst. Growth.* 363, 211 (2013).
56. S. Shettigar, G. Umesh, K. Chandrasekaran, and B. Kalluraya, *J. Synth. Met.* 157, 142 (2007).
57. Y.S. Zhou, E.B. Wang, and J. Peng, *J. Polyhedron.* 18, 1419 (1999).
58. N.Y. Kamber, G. Zhang, S. Liu, S.M. Mikha, and W. Haidong, *J. Opt. Commun.* 184, 475 (2000).
59. M.T. Zhao, B.P. Singh, and P.N. Prasad, *J. Chem. Phys.* 89, 5535 (1988).
60. H.M. Shanshoola, M. Yahaya, W.M.M. Yunus, and I.Y. Abdullah, *J. Teknol.* 78, 33 (2016).
61. H. Fan, Q. Ren, X. Wang, T. Li, J. Sun, G. Zhang, D. Xu, G. Yu, and Z. Sun, *Nat. Sci.* 1, 136 (2009).

Authors and Affiliations

S. Prince[1,2] · T. Suthan[2,3] · C. Gnanasambandam[2,4]

✉ T. Suthan
suthantr@yahoo.co.in

[1] Physics Research Centre, S.T. Hindu College, Nagercoil 629002, India

[2] Affiliated to Manonmaniam Sundaranar University, Abishekapatti, Tirunelveli 627012, India

[3] Department of Physics, Lekshmipuram College of Arts and Science, Neyyoor 629802, India

[4] Department of Physics, S.T. Hindu College, Nagercoil 629002, India